A New Hybrid Kinematic/Dynamic Whole-Body Control for Humanoid Robots With Real-Time Experiments

David Galdeano, Ahmed Chemori, Sébastien Krut, Philippe Fraisse

A New Hybrid Kinematic/Dynamic Whole-Body Control for Humanoid Robots With Real-Time Experiments

D. Galdeano[†], A. Chemori[*†], S. Krut[†] and P. Fraisse[†]

[†] *LIRMM, University of Montpellier, CNRS, Montpellier, FRANCE*

[*] *Corresponding author: Ahmed.Chemori@lirmm.fr*

Received Day Month Year
Revised Day Month Year
Accepted Day Month Year

In this paper, a new hybrid kinematic/dynamic control scheme for humanoid robots is proposed. Its basic idea lies in the tracking of several values in both operational and joint spaces. These values include (i) the relative pose of the robot's feet, (ii) the position of the center of mass, (iii) the body's orientation and (iv) the admissible range of variation of the joints. A zero moment point (ZMP) based dynamic feedback is included in the proposed scheme to improve the stability of dynamic motions. The proposed stabilizer is based on a spherical projection of a nonlinear PID regulation control law. Through the proposed study, it is shown that these objectives allow to produce smooth dynamically stable whole-body motions. The effectiveness and robustness of the proposed control scheme is demonstrated through four real-time experimental scenarios, conducted on HOAP-3 humanoid robot.

Keywords: Whole-body control; Posture control; Hybrid kinematic/dynamic; ZMP regulation; Humanoid robot.

1. Introduction

Humanoid robot walking is still a challenging field of research, due to the inherent difficulties of generating stable dynamic walking gaits for those systems. Within this field, humanoid robots need sophisticated control schemes to deal with their complexity, as well as their evolution environment. The related difficulties in developing such control approaches include, among others:

- The standing position stability is directly related to the feet sizes,
- humanoid robots are usually composed of complex tree-like kinematic structures (or parallels mechanisms [1,2]), with a closed kinematic chain in double support phases, and
- their large number of degrees of freedom making them highly redundant.

The highly redundant nature of humanoid robots can be tackled by whole-body control, which allows the distribution of motion on all the degrees of freedom.

Whole-body controls may lead to more human-like motions than classical control algorithms using only a part of the available degrees of freedom.

In the literature, several approaches have been proposed to deal with whole-body control; they can be mainly classified into two classes: *kinematic whole-body control* and *dynamic whole-body control*.

Kinematic whole-body control can be achieved using a simplified model of the robot. For instance, the widely known Inverted Pendulum Model (IMP) has been proposed by Kajita et al.[3] This method considers the robot as a single point mass with massless legs, simplifying the dynamics of the robot to an inverted pendulum. Since then, many extensions have been proposed, like the Linear Inverted Pendulum Model (LIPM). [4,5,6] These models have been successfully used but are mainly limited to walking tasks.

Another way to achieve a kinematic whole-body control is to use the task framework, as defined by Nakamura and Siciliano, to allow the tracking of several objectives in operational space. [7,8] The tasks-based framework uses only the robot kinematics, which is not adapted to humanoid robots, since their stability is closely related to dynamic parameters such as external and reaction forces applied on the robot. For instance, a humanoid robot control should take into account the contact forces with the ground to create a motion stabilizer [9]. This is why most of the proposed tasks-based studies propose to use a dynamic model of the robot.

Dynamic whole-body control is based on the task formalism using a dynamic model of the robot to compute the necessary control torques and the associated contact efforts. [10,11] The use of a dynamic model may allow to compensate for dynamical effects of the motions to avoid falling down of the robot.

A framework based on dynamic whole-body tasks control has been developed for humanoid robots by Sentis and Khatib for multi-contact dynamic motions.[12] Mansard et al. have created another dynamic whole-body tasks control framework called the stack of tasks. [13] This framework improves dynamic whole-body tasks control by allowing online adding and removal of tasks during the control execution. Furthermore, they have also provided a flexible C++ implementation of the proposed algorithm.

It is worth to note that dynamic whole-body control approaches often need a precise model of the robot and its environment. However, a precise model of the robot is mainly difficult to obtain, since the dynamic effects are highly nonlinear and a precise model of the environment is even harder to produce [14]. For this reason, a reactive approach would be more efficient in a realistic environment. Recently, to provide a certain robustness against unprecise models, some works on inverse-dynamics based torque control using velocity feedback, have been proposed [2] and also proved to be reactive.

In this paper, a new hybrid kinematic/dynamic whole-body control strategy is proposed. The basic idea of this control scheme lies in the kinematic tracking of a desired feet motion and a Center of Mass (CoM) position to produce stable motions. The CoM position tracking is then modified using a zero moment point

(ZMP) based control feedback (the stabilizer) to improves the dynamic stability of the humanoid robot. The result of such consideration is a dynamic feedback used altogether with a kinematic whole-body control, resulting in a scheme reactive to external disturbances.

The proposed whole control scheme is composed of four mains kinematic objectives , including (i) a feet pose tracking, (ii) a CoM position tracking, (iii) a body orientation objective and (iv) joint limits avoidance, to deal with the singularities issue. A stabilizer is then added to ensure the dynamic stability of the robot motions. This stabilizer uses a nonlinear PID regulation controller with a spherical projection of the regulation control law.

In the literature, most of the studies often decompose the walking cycle into several distinct phases and a controller is designed for each phase resulting in switching between these control laws.[15,16,17,18] The usual walking phases are single-support, impact and double-support [19,20]. With our proposal approach, such a decomposition is no more needed. One advantage of our approach lies in its ability to generate a continuous whole-body switching-free control, even when a foot is lifted off from ground or landed. The main contributions of the present paper can be summarized as follows:

(1) The first main contribution is to enable a cyclic pose task for one foot with respect to the other. This idea will help to avoid the decomposition of the walking cycle into single and double support phases. Consequently, this gives the ability to generate a continuous whole-body switching-free control scheme.
(2) The second contribution deals with a sphere-projected ZMP stabilizer embedded in the CoM task, which enables a simple and effective ZMP-based stabilization.
(3) The third contribution is the definition of a metric based on footprints and ZMP measurement to characterize the stability margins. This metric enables a simple stability quantification and can be useful during fine tuning of algorithms.
(4) As a fourth contribution the effectiveness and robustness of the proposed control scheme have been demonstrated through four different real-time experimental scenarios, presented and discussed in the paper.

This paper is organized as follows, in next section, the proposed hybrid kinematic/dynamic control scheme is presented. Real-time experimental results on a humanoid demonstrator are presented and discussed in section 3. The paper ends with some concluding remarks and future work.

2. Proposed Hybrid Kinematic/Dynamic Control Scheme

The main contribution of this work is to propose a kinematic control of the CoM position augmented with a dynamic feedback, resulting in a ZMP regulator, to

improve the dynamic stability of the robot motion. This approach enables to control continuously the evolution of both the CoM and ZMP.

2.1. *Kinematics objectives*

The proposed control scheme relies on four main objectives to produce a whole-body motion including: (i) a relative feet pose tracking, (ii) a center of mass position tracking, (iii) a hip orientation tracking and (iv) joint limits avoidance objective.

These objectives are introduced in the sequel, further information can be found in [21,22,23,24].

2.1.1. *Relative feet pose objective*

The relative feet pose (rfp) objective is designed to track the pose, including the position and orientation, of one foot with respect to the other one (cf. illustration of Fig. 1).

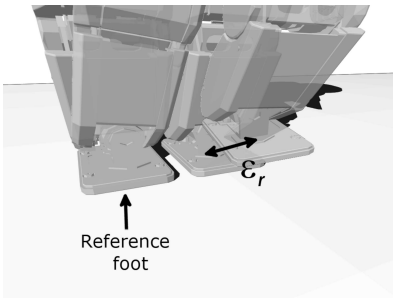

Fig. 1: Illustration of the tracking error on the relative feet pose.

This tracking objective is expressed in the right foot reference coordinate in order to design cyclic walking pattern, independent of the position of the robot in its environment (flat or inclined ground, stairs, etc.).

Let us define the error of the relative feet pose as follows:

$$\varepsilon_r = [E_{pos}^T \; E_{ori}^T]^T \tag{1}$$

where $E_{pos} \in \mathbb{R}^{3\times 1}$ is the Cartesian position error defined in (2) and $E_{ori} \in \mathbb{R}^{3\times 1}$ is the orientation error defined in (3).

The Cartesian position error is define as the displacement between the desired and the real position of the foot w.r.t the other foot. This error can be expressed as:

$$E_{pos} = P_{rd} - P_r \tag{2}$$

where $P_{rd} = [x_{rd}\ y_{rd}\ z_{rd}]^T$ is the desired relative feet position and $P_r = P_{rf} - P_{lf}$ is the real relative feet position with $P_{rf} = [x_{rf}\ y_{rf}\ z_{rf}]^T$ and $P_{lf} = [x_{lf}\ y_{lf}\ z_{lf}]^T$ are respectively the positions of the right and left foot obtained using the forward kinematic model.

The orientation error is define as the difference of orientation between the desired and the real orientation of the foot w.r.t the other foot point of view. This error can be expressed as:

$$E_{ori} = R_{rf}\ (\ln(R_{rf}^{-1}\ R_{lf}\ R_{rd}))^{\vee} \tag{3}$$

where $R_{rd} \in \mathbb{R}^{3\times3}$ is the desired relative feet orientation matrix, $R_{rf} \in \mathbb{R}^{3\times3}$ and $R_{lf} \in \mathbb{R}^{3\times3}$ are respectively the right and left foot orientation matrices obtained from the forward kinematic model. The logarithmic map operator $\omega = (\ln R)^{\vee}$ is defined in authors previous works.[21]

The Jacobian matrix of the relative feet pose is define as follows:

$$\varepsilon_r = J_r \varepsilon_q \tag{4}$$

where $\varepsilon_q \in \mathbb{R}^{n\times1}$ represents the vector of articular position errors of the robot, $J_r \in \mathbb{R}^{6\times n}$ is the Jacobian matrix of the relative feet pose and n denotes the number of degrees of freedom.

2.1.2. *Center of mass position objective*

The Center of Mass (CoM) is a good stability indicator in the case of static motions of humanoid robots and the control of its position has been widely addressed in the literature.[25,26] The CoM position objective is used to improve the stability of the robot motion as well as its performances. It places the CoM position of the robot in the three-dimensional operational space to produce stable motions.

The error of the CoM position is define by:

$$\varepsilon_{CoM} = CoM_d - CoM \tag{5}$$

where $CoM_d = [x_{CoM_d}\ y_{CoM_d}\ z_{CoM_d}]^T$ is the desired position of the center of mass and $CoM = [x_{CoM}\ y_{CoM}\ z_{CoM}]^T$ is the real position of the center of mass obtained using the forward kinematic model of the center of mass.

It is worth to note that CoM_d and CoM needs to be defined in the same coordinate system. We propose to use one foot as the reference coordinate system. This choice will allow the design of cyclic trajectories for the desired CoM position for various periodic motion like walking, without having to refer to a global coordinate system which would need a precise position of the robot in its environment.

The Jacobian matrix of the center of mass position can be defined as follows:

$$\varepsilon_{CoM} = J_{CoM} \varepsilon_q \tag{6}$$

where $J_{CoM} \in \mathbb{R}^{3\times n}$ is the Jacobian matrix of the center of mass position.

2.1.3. *Body orientation objective*

The previous objectives aim to generate a stable walking by using well defined reference trajectories. However, it enables to add some extra aesthetic or functional objectives.

The body orientation objective is used to keep the torso of the robot upright in order to produce more natural motions.

The orientation error of the body, $\varepsilon_{ori} \in \mathbb{R}^3$, is expressed as follows:

$$\varepsilon_{ori} = R_{Ref} \ (\ln(R_{Ref}^{-1} \ R_{Body} \ R_{BodyDes}))^{\vee} \tag{7}$$

where $R_{BodyDes} \in \mathbb{R}^{3\times3}$ denotes the desired body orientation matrix, $R_{Ref} \in \mathbb{R}^{3\times3}$ and $R_{Body} \in \mathbb{R}^{3\times3}$ are respectively the right foot and the body orientation matrices. The orientation is computed in the right foot reference coordinate to allow a simple design of the trajectories. The Jacobian matrix of the body orientation can be defined as follows:

$$\varepsilon_{ori} = J_{ori}\varepsilon_q \tag{8}$$

where $J_{ori} \in \mathbb{R}^{3\times n}$ is the Jacobian matrix of the body orientation.

2.1.4. *Joint limits avoidance objective*

The above objectives are designed to produce whole-body motions; however, due to redundancy there exist more than one admissible configuration which respect the previously defined objectives. Therefore, it is useful to constraint the remaining degrees of freedom to converge to a unique admissible pose.

For instance, for a more stable motion generation, it would be desirable that the robot converges to a comfort posture. To tackle this problem, several studies proposed a joints' limits avoidance objective.[27,28] This objective avoid the drift which may occur when the three previous objectives are respected and some degrees of freedom are left free (due to redundancy). This objective allows, also, to keep the robot away from the limits of its joints which can induce some loss of degrees of freedom (due to singularities).

The joints' limits avoidance objective is based on an attractive potential field that enables to define a comfort position (as illustrated in Fig. 2).[29] This last one is defined with the joints at the farest position from their articular position boundaries.

The attractive potential fields can be defined as follows:

$$\varepsilon_{Joints} = \beta \ [\varepsilon_{q_1} \ \varepsilon_{q_2} \ \varepsilon_{q_3} \ ... \ \varepsilon_{q_{22}}]^T \tag{9}$$

with:

$$\varepsilon_{q_i} = \frac{2 \ (q_i - q_{imed})}{|q_{imax} - q_{imin}|} \quad ; \quad q_{imed} = \frac{q_{imax} + q_{imin}}{2} \tag{10}$$

where $\beta \in \mathbb{R}_+^*$ is a convergence gain, q_{imax} and q_{imin} are respectively the upper and lower limits of the joint i, q_i is position of the current joint i and q_{imed} is its comfort position.

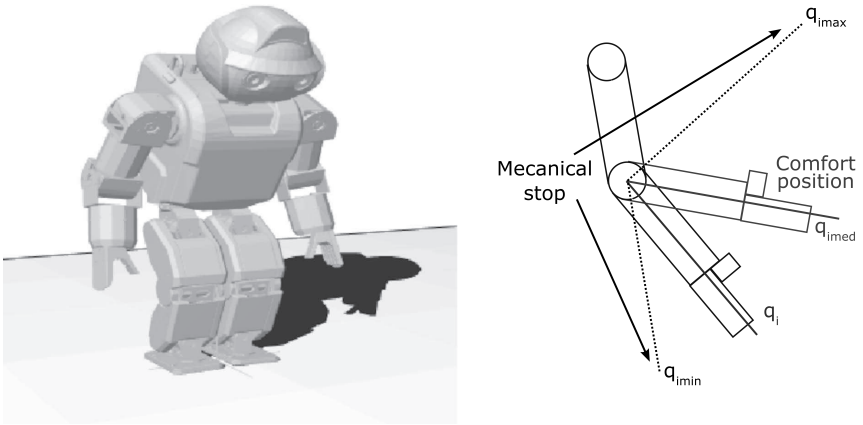

(a) (b)

Fig. 2: The robot's comfort configuration is defined with joint positions far from their limits. (a): Illustration of this comfort configuration on the whole robot, (b): Illustration of the comfort position on one joint.

2.2. *The proposed ZMP-based stabilizer*

In this work, we aim at producing dynamically stable motions. This can be achieved by including a stabilizer to the proposed control scheme, it will be based on a ZMP feedback control.

In [21], the proposed ZMP error compensation was acting directly on the CoM tracking, using a PD controller. This approach was valid for small disturbances during standing or walking on a horizontal flat ground. However, for large ZMP errors, resulting from an inclined ground, the ZMP error can have large amplitudes and should be appropriately managed to avoid unfeasible motions.

To achieve that purpose, we propose to improve the previous work by using a nonlinear PID controller [30,31], coupled with a spherical projection of the regulation.

2.2.1. *Nonlinear PID regulation controller*

Let us define the tracking error on the ZMP position, ε_Z, as follows:

$$dZ_l = Z_{ld} - Z_{lm} \tag{11}$$

$$dZ_r = Z_{rd} - Z_{rm} \tag{12}$$

$$\varepsilon_Z = \alpha \; dZ_l + (1 - \alpha) \; dZ_r \tag{13}$$

$$\alpha = \frac{AZ_r}{AZ_l + AZ_r} \tag{14}$$

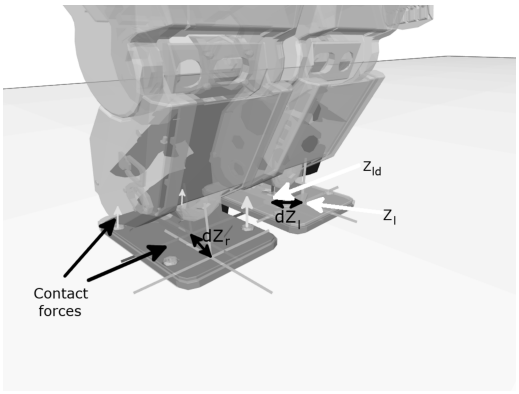

Fig. 3: Graphical illustration of the tracking errors on the ZMP position.

where dZ_l and dZ_r are illustrated in Fig. 3. AZ_l and AZ_r are the amplitudes of the normal contact forces with the ground, applied respectively on the left and the right foot. These values are measured thanks to the four pressure sensors of each foot (cf. green arrows in Fig. 3). $Z_{ld} \in \mathbb{R}^{2\times1}$ and $Z_{rd} \in \mathbb{R}^{2\times1}$ denote the desired positions of the ZMP, under the right and left soles, respectively (i.e. red cross indicated by red arrow in Fig. 3). $Z_{lm} \in \mathbb{R}^{2\times1}$ and $Z_{rm} \in \mathbb{R}^{2\times1}$ are respectively the measured positions of the ZMP, under the right and left soles (blue cross indicated by blue arrow in Fig. 3).

The desired positions of the ZMP, Z_{ld} and Z_{rd}, are chosen to be at the center of each foot ($x\_Z_d = 0$; $y\_Z_d = 0$). These values, reflecting maximum dynamic stability margins, allow to enhance the dynamic stability without a need to generate a complex reference trajectory.

Through equation (13), it can be seen that whenever the robot is in contact with the ground through both feet, the stabilizer uses both feet ZMP errors to produce the dynamic stability regulation. However, when the robot is in contact through one foot only (i.e. single support configurations), the stability controller track only the ZMP of the support leg. This is due to the weighted distribution defined in (14), which imposes a more precise control of the leg which supports most of the weight. This tracking error of the ZMP position is used as input of the proposed nonlinear PID controller.

Nonlinear PID (NPID) control is an improvement of the classical linear PID controller, used in robotics for its robust and reactive behaviour with a favorable damping.[30,31,32,33] With this controller, the system response can be improved in terms of three performance indices, including (i) the stability, (ii) the precision and (iii) the rapidity. This can be achieved thanks to the three control actions of the controller. The NPID uses time-varying gains to improve the control performance.

The control law of the NPID based on the ZMP error ε_Z can be expressed as

follows:

$$u_Z = k_p(\varepsilon_Z)\varepsilon_Z + k_d(\dot{\varepsilon}_Z)\dot{\varepsilon}_Z + k_i \int \varepsilon_Z \tag{15}$$

where $k_p(\varepsilon_Z)$ and $k_d(\dot{\varepsilon}_Z)$ are time-varying proportional and derivative feedback gains; and k_i is a constant integral gain.

The nonlinear proportional feedback gain, illustrated in Fig. 4, is defined as follows:

$$k_p(\varepsilon_Z) = \begin{cases} k_p|\varepsilon_Z|^{\alpha_1 - 1}, & |\varepsilon_Z| > \delta_1, \\ k_p\delta_1^{\alpha_1 - 1}, & |\varepsilon_Z| \leqslant \delta_1. \end{cases} \tag{16}$$

where α_1 is the nonlinearity tuning parameter and δ_1 its threshold of activation.

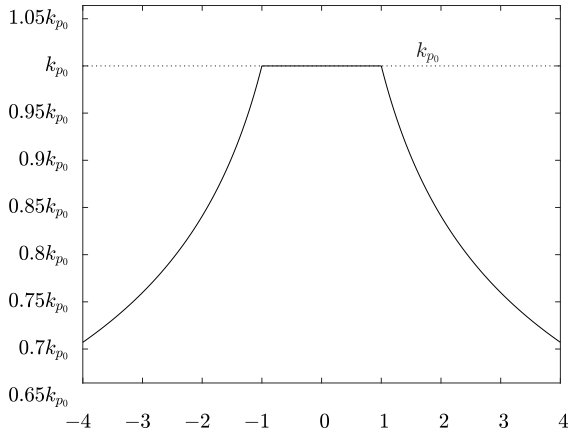

Fig. 4: Illustration of a typical evolution of the nonlinear proportional gain k_p versus the position error e, with $\alpha_1 = 0.75$ and $\delta_1 = 1$.

The nonlinear derivative gain, illustrated in Fig. 5, can be expressed as follows:

$$k_d(\dot{\varepsilon}_Z) = \begin{cases} k_d|\dot{\varepsilon}_Z|^{\alpha_2 - 1}, & |\dot{\varepsilon}_Z| > \delta_2, \\ k_d\delta_2^{\alpha_2 - 1}, & |\dot{\varepsilon}_Z| \leqslant \delta_2. \end{cases} \tag{17}$$

where α_2 represents the nonlinearity tuning parameter and δ_2 its threshold of activation.

The tuning of the gains $\alpha_1 \in [0.5, 1.0]$ and $\alpha_2 \in [1.0, 1.5]$ is performed to produce fast trajectory tracking with improved disturbance rejection, as proposed in Shang and Cong works for the control of parallel robots.[34]

2.2.2. *Spherical projection of the regulation*

In the case of large ZMP disturbances, as those induced by an inclined floors, a simple projection of the ZMP regulator on the CoM tracking transverse plane

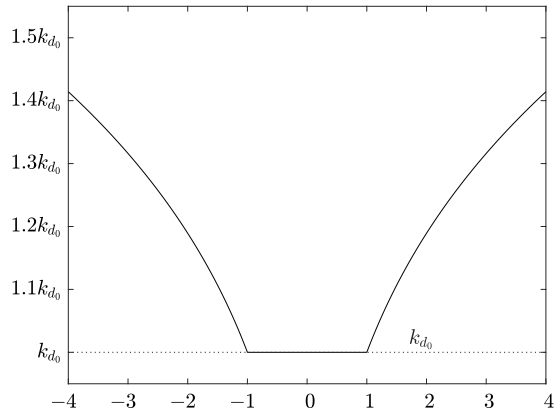

Fig. 5: Illustration of a typical evolution of the nonlinear derivative gain $k_d(\cdot)$ versus the velocity error $\dot{e}$, with $\alpha_2 = 1.25$ and $\delta_2 = 1$.

may produce undesired postures. If the ZMP correction is too large, the desired CoM position is stretched to an unreachable position, creating singularities in the stretched legs. To deal with this issue, we propose to use a spherical projection of the regulation to stay inside a reachable pose space (cf. illustration of Fig. 6).

Assumption 1: In the conducted real-time experiments, the zmp-based controller aims at maintaining a stable posture in standing position. The applied correction is therefore limited to small torso angles (less than 45°) to avoid singularities which may arise form Euler angles transformations.

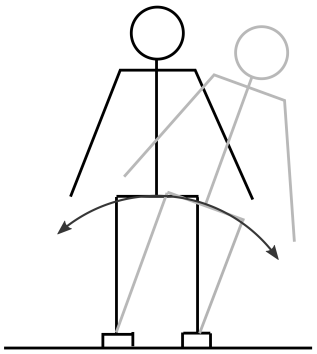

Fig. 6: Frontal view of the spherical projection of the ZMP error with torso orientation compensation.

The spherical operator is based on the projection of the ZMP compensation error on a sphere centered at the middle point between the feet (i.e. the center of the polygon of double support), with a radius equal to the height of the CoM, as illustrated in Fig. 7.

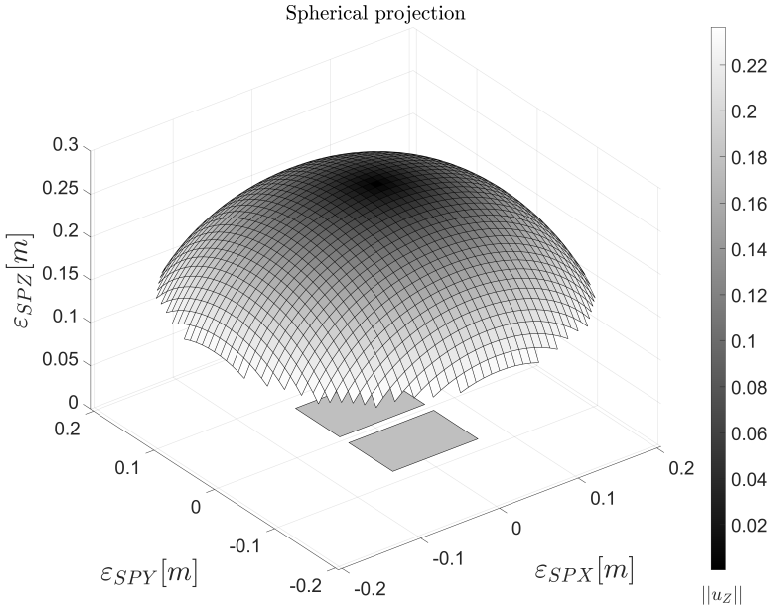

Fig. 7: Illustration of the spherical projection space w.r.t. the norm of u_Z, the footprints are displayed in gray color.

The spherical projection relationship of the ZMP compensation error $\varepsilon_{SP} = [\varepsilon_{SPX} \;\; \varepsilon_{SPY} \;\; \varepsilon_{SPZ}]^T$, with $u_Z = [u_Z(x) \;\; u_Z(y)]^T$ from (15), is expressed as follows:

$$\begin{aligned} \varepsilon_{SPX} &= h_{CoM} \sin\left(\frac{u_Z(x)}{h_{CoM}}\right), \\ \varepsilon_{SPY} &= h_{CoM} \sin\left(\frac{u_Z(y)}{h_{CoM}}\right), \\ \varepsilon_{SPZ} &= h_{CoM} \cos\left(\frac{u_Z(x)}{2h_{CoM}} + \frac{u_Z(y)}{2h_{CoM}} - 1\right). \end{aligned} \tag{18}$$

where h_{CoM} is the initial CoM height.

The spherical projection of the ZMP compensation error is then added to the CoM tracking objective to produce a hybrid kinematic/dynamic tracking:

$$\varepsilon_{CoM\&ZMP} = \varepsilon_{CoM} + \varepsilon_{SP} \tag{19}$$

where $\varepsilon_{CoM\&ZMP}$ is the stability objective containing the CoM tracking and the ZMP regulation; and ε_{CoM} is the CoM tracking error.

The body orientation must also be managed to follow this configuration as illustrated in Fig. 6. The orientation error of the body becomes ε_{ori_sp} and can be defined as follows:

$$\begin{aligned} \varepsilon_{ori\_sp}(r) &= \varepsilon_{ori}(r) + \text{atan2}(u_Z(y), h_{CoM}), \\ \varepsilon_{ori\_sp}(p) &= \varepsilon_{ori}(p) + \text{atan2}(u_Z(x), h_{CoM}), \\ \varepsilon_{ori\_sp}(y) &= \varepsilon_{ori}(y). \end{aligned} \tag{20}$$

where $\varepsilon_{ori}(r)$, $\varepsilon_{ori}(p)$ and $\varepsilon_{ori}(y)$ are respectively the roll, pitch and yaw components of the orientation error of the body. Fig. 6 illustrates a typical reaction of the proposed control scheme in case of an inclined ground or a constant external disturbing force, like a weight modification (e.g. resulting from a payload) for instance.

2.2.3. *Stability analysis*

The dynamic walking stability is closely related to two key notions in humanoid robotics, namely (i) the zero moment point (ZMP) and (ii) the polygon of support. The dynamic walking is stable if the ZMP remains within the polygon of support during the whole walking cycle. Accordingly, this delimits the dynamic stability region whose boundaries are defined by the polygon of support limits (i.e. the contact footprint limits in the single support phase of the walking cycle, for instance). However, if the ZMP is outside the polygon of support, the dynamic walking is unstable and the robot falls down.

This stability concept is illustrated in Figure 8 hereafter, where we can distinguish both the stability and instability regions. Based on this concept we can only conclude if the walking is either stable (green region in Figure 8) or unstable (red hatching region in Figure 8), but we cannot quantify the degree of stability.

To go further, beyond this all-or-nothing concept of stability, it would be interesting to quantify the degree of stability. To this end, we propose to define the stability margins. These metrics will help us to measure and quantify how far we are from the instability limits.

This proposed tool can be used to analyse the dynamic stability as well as to quantify the degree of this stability. The more far we are from these limits the better stability is. Consequently, these metrics can be used to improve the dynamic walking stability if we can increase the stability margins (through trajectory generation and/or optimization, control design, etc.).

These stability margins are illustrated in Figure 9 hereafter, where the dashed red interior rectangle defines the boundaries of the ZMP displacements.

Based on the illustration of Figure 9, the stability margins can be computed as

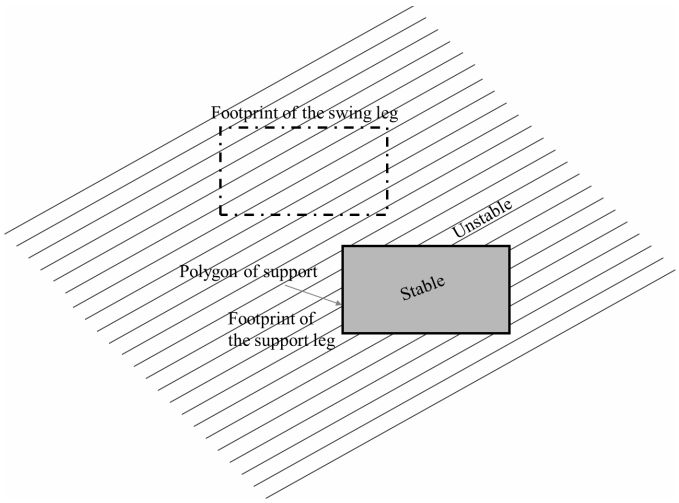

Fig. 8: Illustration of the stability and instability regions, based on the location of the ZMP.

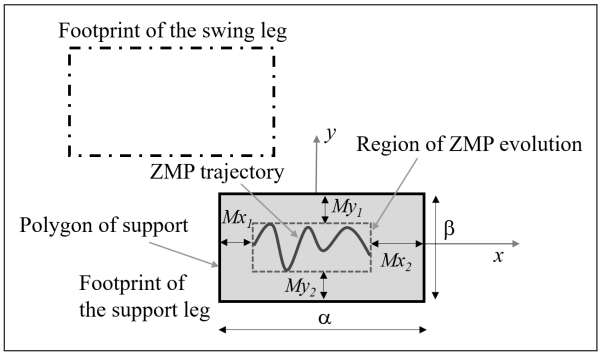

Fig. 9: Illustration of the stability margins.

follows:

$$Mx_1 = \frac{\alpha}{2} + Min(dZMP_x(t)),\ Mx_2 = \frac{\alpha}{2} - Max(dZMP_x(t))$$
$$My_1 = \frac{\beta}{2} + Min(dZMP_y(t)),\ My_2 = \frac{\beta}{2} - Max(dZMP_y(t))$$
$$for\ all \quad t \in [ts_i\ ,\ ts_f]$$
$$Mx = Min(Mx_1, Mx_2),\ My = Min(My_1, My_2)$$

were $dZMP_x(t)$ and $dZMP_y(t)$ are the deviations of the ZMP trajectory with respect to the center of the stance foot along x and y axes respectively, ts_i and ts_f are times of landing and lift-off of the stance foot respectively.

2.3. *Overall architecture of the proposed control scheme*

In the field of motion generation for humanoid robots, whole-body motion generation remains an open problem. One of the promising solutions to track several objectives in operational space is to use the task based formalism. The first use of a task-like control law has been proposed by Liegeois in 1977 and applied to a six-degree-of-freedom (dof) robotic arm to control the end-effector position, while avoiding the joint limits.[29] This approach has been later extended by Nakamura and Siciliano to allow multiples objectives to be tracked by a robotic arm, where they considered a task of obstacle avoidance.[7,8] Later, a task-oriented dynamic control has been proposed by Sentis and Khatib to take into account the dynamics of the robot and was applied to a humanoid robot.[12] Recently, Mansard has developed and standardized a hierarchical task approach for humanoid robots to allow dynamic adding and removal of tasks during the motion execution.[35,13]

The main contribution of the present paper lies in the proposition of a hybrid kinematic/dynamic whole-body control architecture. A kinematic hierarchical task whole-body control is used to track (i) the relative feet pose, (ii) the CoM position, (iii) the body orientation and (iv) avoid the joint limits; this architecture is extended with a dynamic feedback based on a ZMP regulation to improve the dynamic stability of robot's motions. It is worth to note that additional tasks such as aesthetics, manipulation or Human-Robot Interaction (HRI) can easily be added with the proposed hierarchical task-based formalism. The robot motion is generated using the control scheme summarized in Fig. 10. This control algorithm is based on the Siciliano's hierarchical task recursive formulation.[8]

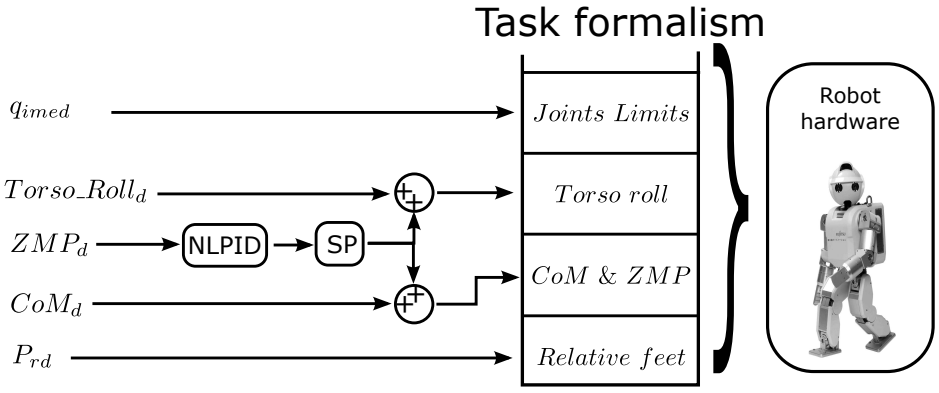

Fig. 10: Block diagram of the proposed control scheme with the hierarchy of objectives. NLPID stands for nonlinear PID and SP stands for spherical projection.

As the objectives are hierarchical, an order of priority among the objectives has to be defined. The objective with the higher priority is the relative feet pose

tracking, since a little error on the feet orientation forbids a double-support pose. With a correct placement of the feet, most motions can be designed to be stable. The control law for one objective, here the relative feet pose, can be expressed as follows:

$$\varepsilon_{q1} = J_r^+ \varepsilon_r \tag{21}$$

where ε_{q1} denotes the displacement to apply on the joint position, J_r and ε_r were defined in section 2.1.1.

The second objective is the CoM position tracking with the ZMP regulation (i.e. the stabilizer). This objective comes in second, since small errors on CoM position can be compensated without a loss of the dynamic equilibrium. The equilibrium of the robot remains a major objective of the robot control, therefore it would be better to add it before any aesthetic or non vital objective. The control law with these two objectives becomes ε_{q2}, expressed by:

$$\varepsilon_{q2} = \varepsilon_{q1} + (\widetilde{J}_{CoM})^+ (\varepsilon_{CoM\&ZMP} - J_{CoM}\varepsilon_{q1}) \tag{22}$$

with:

$$\widetilde{J}_{CoM} = J_{CoM} P_r \quad \text{and} \quad P_r = (\mathbb{I} - J_r^+ J_r) \tag{23}$$

If other objectives are necessary, they can be inserted at this hierarchical level using Siciliano's hierarchical tasks recursive formulation [8]. Possible desired objectives may include objects manipulation, Human-robots interaction (HRI) or an aesthetical tasks like upper-body and head orientations. For instance, the body orientation objective is added here as a third priority task. The associated control law is described by the following expression:

$$\varepsilon_{q3} = \varepsilon_{q2} + (\widetilde{J}_{ori})^+ (\varepsilon_{ori\_sp} - J_{ori}\varepsilon_{q2}) \tag{24}$$

with:

$$\widetilde{J}_{ori} = J_{ori} P_{CoM} \quad \text{and} \quad P_{CoM} = (P_r - \widetilde{J}_{CoM}^+ \widetilde{J}_{CoM}) \tag{25}$$

The objective with the lowest priority should be the joint limits avoidance objective, since it deals with articular limits and singularities. This should always be added as the lowest priority objective since no other objectives can be added after this last one. This is due to the fact that the joint limits avoidance objective is a task in the joint space, i.e. applied to every joint; consequently, the null-space of the control is full. The final resulting control law can be expressed as follows:

$$\varepsilon_{q4} = \varepsilon_{q3} + (P_{ori})^+ (\varepsilon_{Joints} - \varepsilon_{q3}) \tag{26}$$

with:

$$P_{ori} = (P_{CoM} - \widetilde{J}_{ori}^+ \widetilde{J}_{ori}) \tag{27}$$

This final resulting control law allows the generation of continuous dynamically stable whole-body motions. This continuity is guaranteed, since neither phases decomposition (i.e. single and double support phases in walking motions), nor switching is used.

3. Experimental Validation on HOAP-3 Humanoid Robot

3.1. *Description and Modeling of HOAP-3*

Our demonstrator, for the proposed control solution, is the HOAP-3 humanoid robot manufactured by Fujitsu company (illustrated in Fig. 11-(a)). The whole experimental setup, used for the forthcoming validation scenarios, consist in (i) the HOAP-3 robot itself, communicating with (ii) a host control PC, and (iii) its evolution environment.

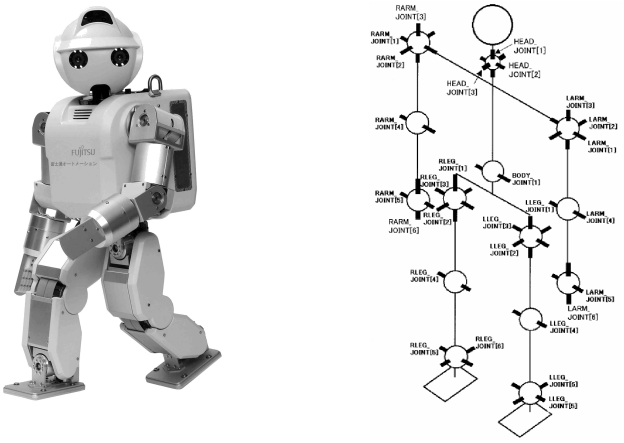

(a) View of HOAP-3 robot

(b) Schematic view of HOAP-3 robot kinematics

Fig. 11: Illustration of HOAP-3 humanoid robot used as a demonstrator for real-time experiments.

The HOAP-3 humanoid robot is a whole-body testbed for humanoid robotic studies. This robot has 60 cm tall, 8.8 kg weight, and n dof ($n = 28$), distributed as follows: Each leg is composed of six dof, three dof at the hip, one dof at the knee and two dof at the ankle. The torso is composed of one dof and the neck is composed of three dof. Both arms are composed of six dof, three dof at the shoulder, one dof at the elbow and two dof at the hand. The spatial distribution of the different dof is illustrated in Fig. 11-(b).

The robot is equipped with optical incremental encoders at all the joints, a 3-axis accelerometer and 3-axis gyroscope are used for posture sensing, four force sensors per foot are used for the measurement of the contact forces with the ground. The robot is also equipped with two cameras for visual feedback.

The actuators of the robot are brushless motors paired with micro-controllers,

which are controlled by an embedded PC running with a real time kernel RT-Linux at a sample frequency of 1 kHz.

To validate the proposed control scheme, four experimental scenarios have been conducted, including (i) the stability improvement scenario, (ii) the online adaptation toward a ground slope variation scenario, (iii) the walking on an irregular ground scenario, and (iv) the walking with an extra weight attached to the arm scenario.

3.2. *Validation 1: Stability improvement*

The proposed control scheme implemented on the HOAP-3 robot has been tested with and without the ZMP regulation to demonstrate the efficiency of the proposed stabilizer.

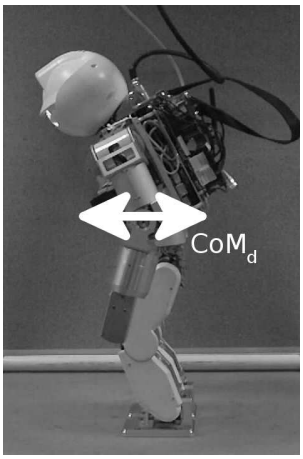

Fig. 12: Illustration of the idea of generation of unstable motions on Hoap-3 humanoid robot to show the effectiveness of the proposed ZMP-based regulator.

The desired relative feet pose is set to be constant. The desired center of mass position is moved forward and backward using a sinus signal with an amplitude increasing over time to produce an unstable motion (cf. illustration of Fig. 12) until the fall of the robot.

For a sinusoidal CoM motion of a period of 1.5 seconds, the robot falls down when the amplitude reaches 21.7 centimeters without the stabilizer and 25.2 centimeters with the stabilizer.

The obtained results show that the proposed stabilizer improves the stability margins of the robot motions, allowing therefore faster motion executions and a wider region of stability.

3.3. *Validation 2: Online adaptation toward a ground slope variation*

The objective of the second validation scenario is to demonstrate the adaptation of the proposed control scheme towards a variation in the slope of the ground.

The experimental environment for this consists of a wooden board (as illustrated in fig 13) which is progressively lifted from one side, therefore creating a rotation around the other side of the board. The desired ZMP is kept constant and located in the middle of the polygon of support, formed by the feet in contact with the ground.

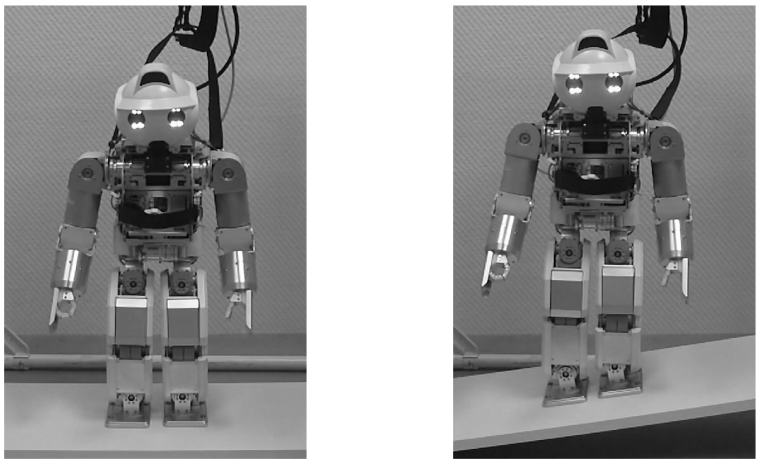

(a) Experimental setup for the second validation

(b) Large ground's inclination

Fig. 13: Illustration of the real-time adaptation against ground's inclination variation. (a): the initial configuration for a zero slope of the ground, (b): the automatic new configuration to compensate the ground inclination and keep the robot stable.

The robot adaptation to the ground's slope variation can be clearly observed on the illustration of Fig. 13(b).

In Fig. 14, the evolution of the CoM position expressed in the right foot's reference frame is displayed. Along the x axis, the trajectory is constant since no perturbation on this axis has been applied. Along the y axis, the trajectory of the desired CoM is kept constant. The observed variation is due to the compensation by the stabilizer of the ZMP displacement. Along the z axis, the trajectory is also kept constant at the height of the initial CoM position.

In Fig. 15, the evolution of the measured ZMP and CoM positions are plotted with respect to footprints of the robot. The variation of the CoM position trajectories are due to the ZMP based compensation.

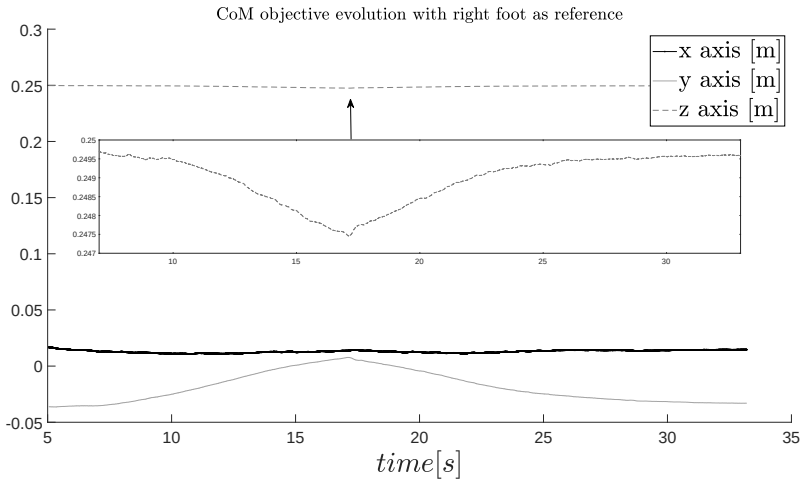

Fig. 14: Evolution versus time of the trajectories of the CoM for the second experimental validation.

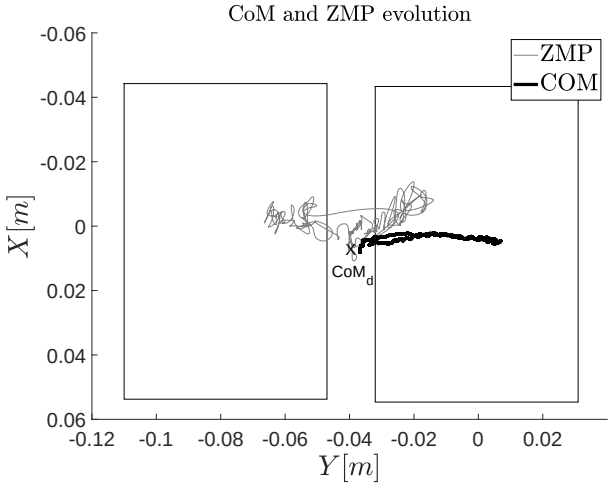

Fig. 15: Evolution of the CoM and ZMP trajectories within the polygon of support composed by footprints for the second experimental validation.

The robot's body adapts quickly its configuration with respect to the variation in the ground slope. The combination of the CoM position adjustment and the hip rotation allows a smooth, natural looking motion.

In Fig. 16, the stability margins Mx and My are depicted versus time. It is worth to note that the minimum values of these stability margins are respectively

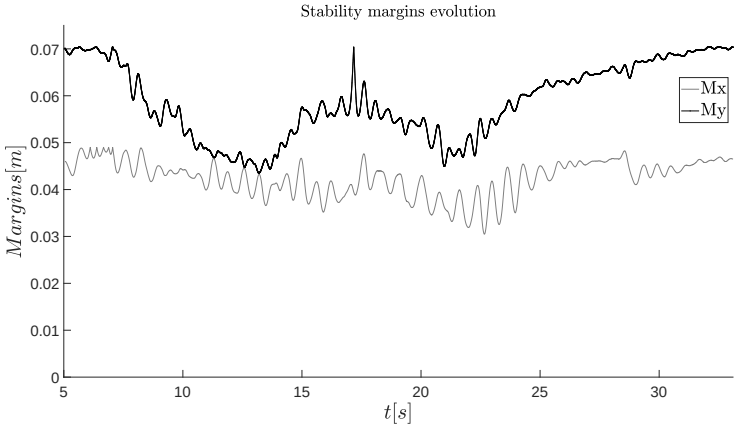

Fig. 16: Evolution versus time of the stability margins Mx and My for the second experimental validation.

given by $Mx_{min} = 3.05\,cm$ and $My_{min} = 4.35\,cm$. Those positive values clearly attest of the guaranteed dynamic stability for the motions of this scenario.

3.4. *Validation 3: Walking on an irregular ground*

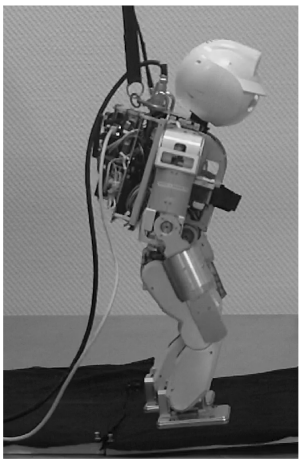

Fig. 17: Illustration of the scenario of walking on an irregular ground, including a horizontal part, followed by an unexpected longitudinal slope.

In the third experiment, the robot is controlled to be walking on a flat ground followed by an unexpected slope of five degrees as illustrated in Fig. 17. The ob-

jective of this scenario is to show the robustness of the control scheme against irregularities in the ground.

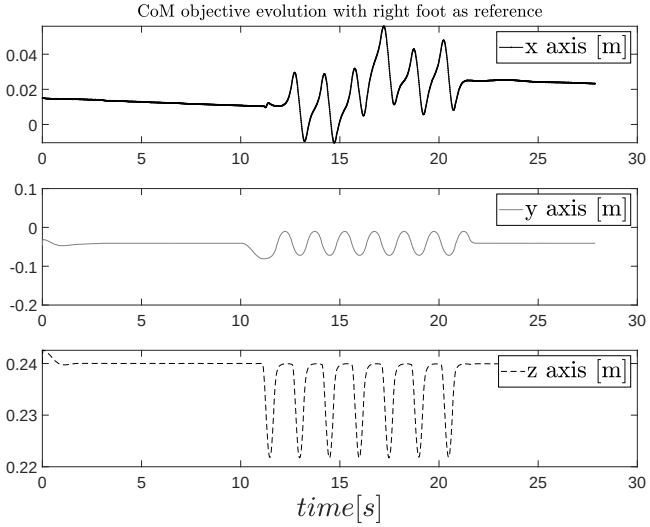

Fig. 18: CoM trajectories evolution with right foot as reference for the third experimental scenario.

In Fig. 18, the evolution of the CoM position expressed in the right foot reference frame is displayed. On the x axis, the ZMP regulation shifts the CoM to maintain the dynamic stability of the robot when walking on the inclined floor.

In Fig. 19, the evolution of the ZMP and the CoM positions are plotted within the polygon of support formed by the footprints of the humanoid robot.

In Fig. 20, the stability margins Mx and My are plotted versus time. It is worth to note that the minimum values of these stability margins are respectively given by $Mx_{min} = 3.24\,cm$ and $My_{min} = 1.79\,cm$. The obtained positive minimal margins are clearly an indicator of a guaranteed dynamic stability of the motions of this scenario.

It is worth to note that the obtained walking motion is stable and robust, where the robot effectively produces the desired walking pattern. Furthermore, it is important to note that, for the same scenario, the robot falls down without the proposed stabilizer. This illustrates clearly the importance and efficiency of the proposed stabilizer.

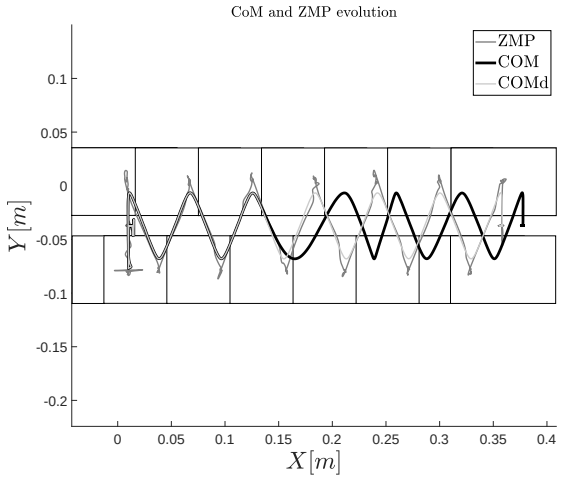

Fig. 19: Evolution of ZMP, CoM and desired CoM trajectories with footprint displayed for the third experimental scenario.

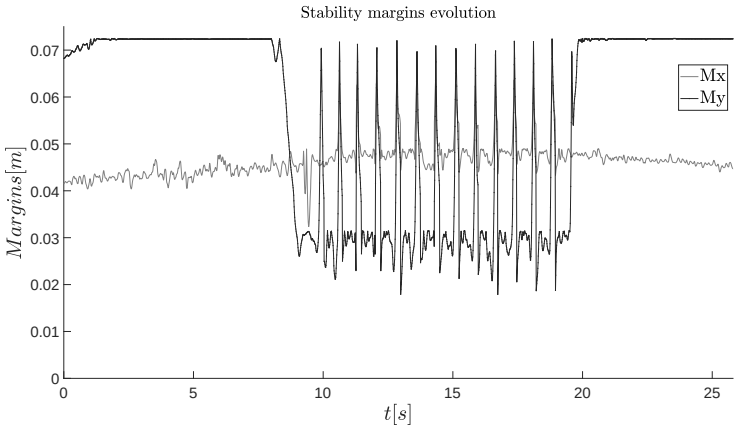

Fig. 20: Evolution versus time of the stability margins Mx and My for the third experimental validation.

3.5. *Validation 4: Walking with an extra weight attached to the arm*

In the fourth experimental scenario, the robot is controlled to be walking on a flat ground with a 0.5 kilograms weight (equal to 5.6% of the robot's total weight) attached to one of its arms as illustrated in Fig. 21. The objective of this validation is to show the robustness of the control scheme against external disturbances, resulting

from the added weight.

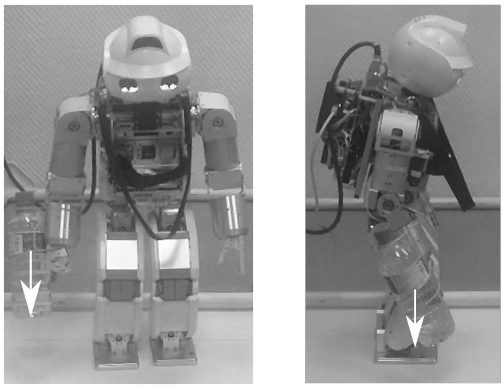

Fig. 21: Illustration of the scenario involving a permanent disturbing force (i.e. the gravity force of a full bottle, oriented as indicated by the green arrow), generated by an extra weight attached to the right arm of the robot.

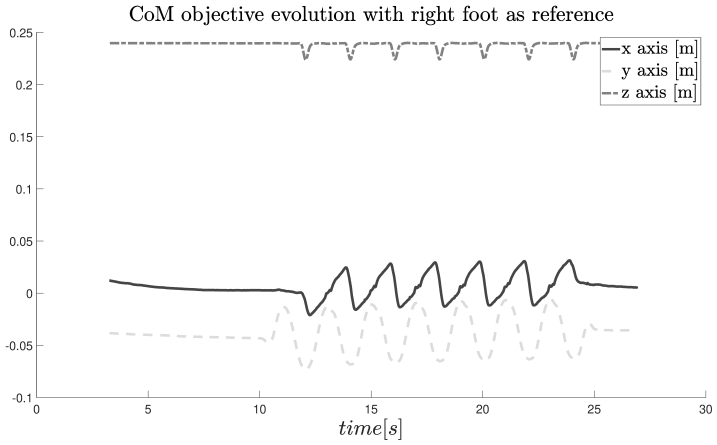

Fig. 22: CoM trajectories evolution with right foot as reference for the fourth experimental scenario.

In Fig. 22, the evolution of the CoM position expressed in the right foot reference frame is displayed. On the y axis, the ZMP regulation shifts the CoM to maintain the stability of the robot walking with the weight attached to the arm.

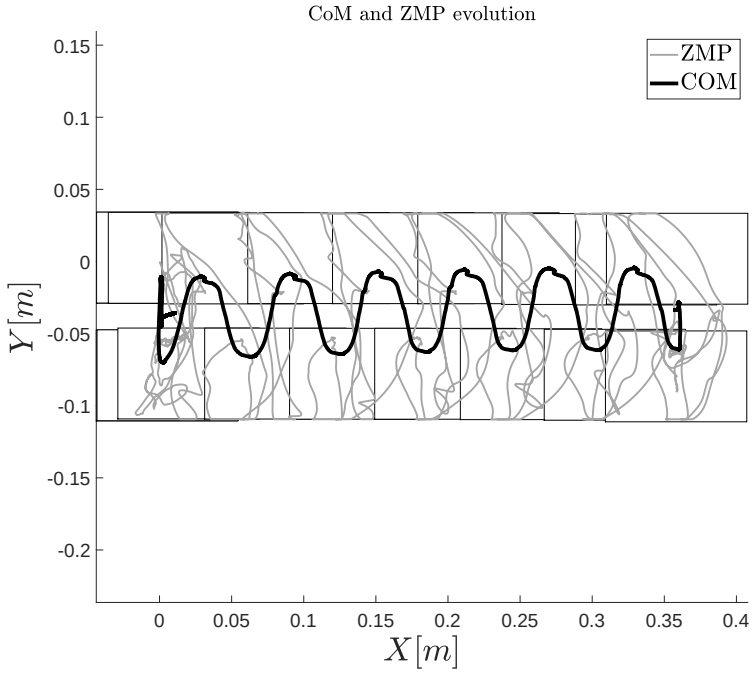

Fig. 23: Evolution of ZMP and CoM trajectories with footprint displayed for the fourth experimental scenario.

In Fig. 23, the evolution of the ZMP position and the CoM position are plotted with respect to footprints of the humanoid robot.

The obtained walking motion is stable and robust. The robot produces effectively the desired walking pattern. It is worth to note that the robot falls down for the same scenario without the proposed stabilizer.

4. Conclusion and Future Work

This paper deals with the generation of dynamically stable whole-body motions. The proposer control scheme is obtained by using a hybrid kinematic/dynamic tracking control with mainly four objectives controlling (i) the relative pose between the feet of the robot, (ii) the trajectory of its CoM, (iii) its body orientation and (iv) the avoidance of joints' limits. A dynamic feedback is added to improve the stability of the motion. This stabilizer is based on a spherical projection of the nonlinear PID regulator.

The main advantage of the proposed control framework is that the generated motion are based on a unique control law, without any need of phase decomposition and the whole generated motion is continuous and more human-like.

In future work, we aim to design some different optimal trajectories for the objectives, to produce human-robot interaction and manipulation tasks.

Acknowledgements

This research was supported by the French National Research Agency, within the project R2A2 (ANR-09-SEGI-011).

References

1. R. J. Saltaren, J. M. Sabater, E. Yime, J. M. Azorin, R. Aracil, and N. Garcia, Performance evaluation of spherical parallel platforms for humanoid robots, *Robotica*, **25**(3), 257–267, (2006).
2. S. Faraji, L. Colasanto, and A. J. Ijspeert, Practical considerations in using inverse dynamics on a humanoid robot: Torque tracking, sensor fusion and cartesian control laws, in *IEEE/RSJ Int. Conf. on Intelligent Robots and Systems (IROS)* (IEEE Press, Hamburg, Germany, 2015), pp. 1619–1626.
3. S. Kajita, F. Kanehiro, K. Kaneko, K. Fujiwara, K. Harada, K. Yokoi, and H. Hirukawa, Biped walking pattern generation by using preview control of zero moment point, in *IEEE Int. Conf. Robotics and Automation (ICRA)* (IEEE Press, Taipei, Taiwan, 2003), pp. 1620-1626.
4. S. Kajita, F. Kanehiro, K. Kaneko, K. Yokoi, and H. Hirukawa, The 3d linear inverted pendulum mode: A simple modeling for a biped walking pattern generation, in *IEEE/RSJ Int. Conf. on Intelligent Robots and Systems (IROS)* (IEEE Press, Maui, Hawaii, USA, 2001), pp. 239–246.
5. S. Kajita, M. Morisawa, K. Miura, S. Nakaoka, K. Harada, K. Kaneko, F. Kanehiro, and K. Yokoi, Biped walking stabilization based on linear inverted pendulum tracking, in *IEEE/RSJ Int. Conf. on Intelligent Robots and Systems (IROS)* (IEEE Press, Taipei, Taiwan, 2010), pp. 4489–4496.
6. X. Xiong and A. D. Ames, Orbit characterization, stabilization and composition on 3d underactuated bipedal walking via hybrid passive linear inverted pendulum model, in *IEEE/RSJ Int. Conf. on Intelligent Robots and Systems (IROS)* (IEEE Press, Macau, China, 2019), pp. 4644–4651.
7. Y. Nakamura, H. Hanafusa, and T. Yoshikawa, Task-priority based redundancy control of robot manipulators, *The International Journal of Robotics Research*, **6**(2), 3–15, (1987).
8. B. Siciliano and J. Slotine, A general framework for managing multiple tasks in highly redundant robotic systems, in *IEEE International Conference on Advanced Robotics (ICAR)* (IEEE Press, Pisa, Italy , 1991), pp. 1211–1216.
9. A. Chemori, S. Le Floch, S. Krut, and E. Dombre, A control architecture with stabilizer for 3d stable dynamic walking of sherpa biped robot on compliant ground, in *IEEE-RAS International Conference on Humanoid Robots* (IEEE Press, Nashville, USA, 2010), pp. 480–485.
10. C.-L. Fok, G. Johnson, J. D. Yamokoski, A. Mok, and L. Sentis, ControlIt! – a software framework for whole-body operational space control, *International Journal of Humanoid Robotics*, **13**(1), 1550040, (2015).
11. P. M. Wensing and D. E. Orin, Improved computation of the humanoid centroidal dynamics and application for whole-body control, *International Journal of Humanoid Robotics*, **13**(1), 1550039, (2016).

12. L. Sentis and O. Khatib, A whole-body control framework for humanoids operating in human environments, in *IEEE Int. Conf. Robotics and Automation (ICRA)* (IEEE Press, Orlando, Florida, USA, 2006), pp. 2641–2648.
13. N. Mansard, O. Khatib, and A. Kheddar, A unified approach to integrate unilateral constraints in the stack of tasks, *IEEE Transactions on Robotics*, **25**(3), 670–685, (2009).
14. P. A. Bhounsule and K. Yamane, Accurate task-space tracking for humanoids with modeling errors using iterative learning control, *International Journal of Humanoid Robotics*, **14**(3), 1750015, (2017).
15. M. A. Hopkins, A. Leonessa, B. Y. Lattimer, and D. W. Hong, Optimization-based whole-body control of a series elastic humanoid robot, *International Journal of Humanoid Robotics*, **13**(1), 1550034, (2016).
16. K. N. Lee and Y. J. Ryoo, Walking pattern tuning system based on zmp for humanoid robot, *International Journal of Humanoid Robotics*, **11**(4), 1442001, (2014).
17. J.-Y. Kim and Y.-S. Kim, Zmp tracking control of an android robot leg on slope-changing ground using disturbance observer and dual plant models, *International Journal of Humanoid Robotics*, **13**(3), 1550043, (2016).
18. S.-J. Yi, B.-T. Zhang, D. Hong, and D. D. Lee, Whole-body balancing walk controller for position controlled humanoid robots, *International Journal of Humanoid Robotics*, **13**(1), 1650011, (2016).
19. A. Chemori and A. Loria, Control of a planar five link under-actuated biped robot on a complete walking cycle, in *the 41st IEEE Conference on Decision and Control (CDC)* (IEEE Press, Las Vegas, NV, USA, 2002), pp. 2056–2061.
20. A. Chemori and A. Loria, Walking control strategy for a planar under-actuated biped robot based on optimal reference trajectories and partial feedback linearization, in *the Fourth International Workshop on Robot Motion and Control (RoMoCo)* (Poznan, Poland, 2004), pp. 61–66.
21. D. Galdeano, A. Chemori, S. Krut, and P. Fraisse, Task-based whole-body control of humanoid robots with zmp regulation, real-time application to a squat-like motion, in *11th edition of the International Multi-Conference on Systems, Signals and Devices (SSD 2014)* (Castelldefels-Barcelona, Spain, 2014), pp. 1–6.
22. D. Galdeano, A. Chemori, S. Krut, and P. Fraisse, Optimal Pattern Generator For Dynamic Walking in humanoid Robotics, in *10th International Multi-Conferences on Systems, Signals and Devices (SSD13)* (Hammamet, Tunisia, 2013), pp. 1–6.
23. D. Galdeano, V. Bonnet, M. Bennehar, P. Fraisse, and A. Chemori, Partial human data in design of human-like walking control in humanoid robotics, in *10th International IFAC Symposium on Robot Control (SYROCO'12)* (Dubrovnik - Croatia, 2012), pp. 485–490.
24. D. Galdeano, A. Chemori, S. Krut, and P. Fraisse, A nonlinear PID stabilizer with spherical projection for humanoids: From concept to real-time experiments, in *IEEE-RAS International Conference on Humanoid Robots* (IEEE Press, Madrid, Spain, 2014), pp. 693–698.
25. F.-J. Montecillo-Puente, M. N. Sreenivasa, and J.-P. Laumond, On real-time whole-body human to humanoid motion transfer, in *International Conference on Informatics in Control, Automation and Robotics (ICINCO'10)* (IEEE Press, Madeira, Portugal, 2010), pp. 22–31.
26. F. Sygulla, R. Wittmann, P. Seiwald, A.-C. Hildebrandt, D.Wahrmann, and D. Rixen, Hybrid position/force control for biped robot stabilization with integrated center of mass dynamics, in *IEEE-RAS International Conference on Humanoid Robots* (IEEE Press, Madrid, Spain, 2017), pp. 742–748.

27. Y. Mezouar and F. Chaumette, Path planning for robust image-based control, *IEEE Transactions on Robotics and Automation*, **18**(4), 534–549, (2002).
28. V. Mohan, P. Morasso, G. Metta, and G. Sandini, A biomimetic, force-field based computational model for motion planning and bimanual coordination in humanoid robots, *Autonomous robots*, **27**(3), 291–307, (2009).
29. A. Liegeois, Automatic supervisory control of the configuration and behavior of multibody mechanisms, *IEEE Transactions on Systems, Man and Cybernetics*, **7**(12), 868–871, (1977).
30. H. Seraji, A new class of nonlinear pid controllers with robotic applications, *Journal of Robotic Systems*, **15**(3), 161–181, (1998).
31. Y. Su, D. Sun, and B. Duan, Design of an enhanced nonlinear pid controller, *Journal of Robotic Systems*, **15**(8), 1005–1024, (2005).
32. Y. Xu, J. Hollerbach, and D. Ma, A nonlinear pd controller for force and contact transient control, *IEEE Control Systems*, **15**(1), 15–21, (1995).
33. H. Saied, A. Chemori, M. Bouri, M. El Rafei, C. Francis, and F. Pierrot, A new time-varying feedback rise control for second-order nonlinear mimo systems: theory and experiments, *International Journal of Control*, **94**(8), 2304–2317, (2021).
34. W. Shang and S. Cong, Nonlinear computed torque control for a high-speed planar parallel manipulator, *Mechatronics*, **19**(6), 987–992, (2009).
35. N. Mansard, O. Stasse, P. Evrard, and A. Kheddar, A versatile generalized inverted kinematics implementation for collaborative working humanoid robots: The stack of tasks, in *IEEE International Conference on Advanced Robotics (ICAR)* (IEEE Press, Pisa, Italy , 2009), pp. 1–6.

David Galdeano received the M.Sc. and Ph.D. degrees both in Robotics and Automation from the University Montpellier 2, France in 2010 and 2014 respectively. He has been a Postdoctoral fellow with the Joint Japanese-French Robotics Laboratory (JRL) in Tsukuba, Japan in 2015. He is currently a project leader in autonomous driving sensors development in Continental Automotive France. His current research interests include autonomous driving, humanoid robotics, whole-body posture control.

Ahmed Chemori received the M.Sc. and Ph.D. degrees both in automatic control from the Grenoble Institute of Technology, Grenoble, France, in 2001 and 2005, respectively. He has been a Postdoctoral Fellow with the Automatic Control Laboratory, Grenoble, France, in 2006. He is currently a tenured Research Scientist in automatic control and robotics with the Montpellier Laboratory of Informatics, Robotics, and Microelectronics.His research interests include nonlinear, adaptive, and predictive control and their applications in wearable robotics, humanoid robotics, underactuated systems, parallel robotics and underwater

Sébastien Krut received the M.Sc. degree in mechanical engineering from the Pierre and Marie Curie University, Paris, France, in 2000 and the Ph.D. degree in automatic control from the Montpellier University of Sciences, Montpellier, France, in 2003. He has been a Postdoctoral fellow with the Joint Japanese-French Robotics Laboratory (JRL) in Tsukuba, Japan in 2004. He is currently a tenured research scientist in Robotics for the French National Centre for Scientific Research (CNRS), at the Montpellier Laboratory of Computer Science, Microelectronics and Robotics LIRMM), Montpellier, France. His research interests include design and control of robotic systems.

Philippe Fraisse received M.Sc. degree in Electrical Engineering from Ecole Normale Superieure de Cachan in 1988. He received Ph.D. degree in Automatic Control in 1994. He is currently Professor at the University of Montpellier, France. He is the head of robotics department (LIRMM) and co-chair of French National Workgroup (GDR Robotique) working on Humanoid Robotics (GT7). He is also member of JRL-France scientific board (Japanese- French joint Laboratory for Robotics, AIST-JRL) and member of IEEE. His research interests include modeling and control applied to robotic and rehabilitation fields, including humanoid robotics, robotics for rehabilitation.